

Electronic magnetization of a quantum point contact measured by nuclear magnetic resonance

Minoru Kawamura,^{1,*} Keiji Ono,¹ Peter Stano,¹ Kimitoshi Kono,¹ and Tomosuke Aono²

¹*RIKEN Center for Emergent Matter Science, Wako 351-0198, Japan*

²*Department of Electrical and Electronic Engineering, Ibaraki University, Hitachi 316-8511, Japan*

(Dated: November 8, 2018)

We report an electronic magnetization measurement of a quantum point contact (QPC) based on nuclear magnetic resonance (NMR) spectroscopy. We find that NMR signals can be detected by measuring the QPC conductance under in-plane magnetic fields. This makes it possible to measure, from Knight shifts of the NMR spectra, the electronic magnetization of a QPC containing only a few electron spins. The magnetization changes smoothly with the QPC potential barrier height and peaks at the conductance plateau of $0.5 \times 2e^2/h$. The observed features are well captured by a model calculation assuming a smooth potential barrier, supporting a no bound state origin of the 0.7 structure.

Quantum point contact (QPC) is a short one-dimensional (1D) channel connecting two electron reservoirs. Its conductance is quantized to integer multiples of $2e^2/h$, where e is electron charge and h is Planck's constant[1, 2]. The conductance quantization is well understood within a model of non-interacting electrons[3]. However, experiments have shown an additional conductance feature, a shoulder-like structure at around $0.7 \times 2e^2/h$ termed as 0.7 structure[4, 5]. Despite the simplicity of a QPC, a comprehensive understanding of the 0.7 structure is still lacking [6–19].

Theories proposed to explain the 0.7 structure can be discriminated according to their predictions on the electron spin arrangement, which include spontaneous spin polarization[6, 7], antiferromagnetic Wigner crystal[8], Kondo screening[9–11], and local spin fluctuations accompanied by van Hove singularity[12, 13]. Especially in the Kondo scenario, the existence of a localized magnetic moment in the QPC is an inevitable ingredient. On one hand, early experiments observing Fano resonances suggested such presence of a local single spin trapped in a bound state regardless of magnetic fields[14]. On the other hand, an experiment measuring compressibility contradicts such bound state formation[18]. Thus, the degree of spin polarization of a QPC is one of the central issues to understand the origin of the 0.7 structure.

However, most experiments[4, 5, 14–17] to date have focused on transmission properties, without the QPC spin polarization being addressed directly. Despite the recent progress in magnetic sensors[20], the magnetization measurement of a QPC containing only a few electrons is still very challenging. Recently, small magnetizations of two-dimensional electron systems (2DESs) embedded in GaAs have been measured[21–23] by combining techniques of current-induced nuclear spin polarization [24–28] and resistance (conductance) detection of nuclear magnetic resonance (NMR) signals of Ga and As nuclei[27–29]. Because of the hyperfine interaction between electronic and nuclear spins, an electronic magnetization produces an effective magnetic field for nuclei,

resulting in the shift of the NMR frequency, the Knight shift. From the Knight shift, the electronic magnetization can be determined[30].

A recent transport experiment by Ren *et al.*[31] suggests such influence of nuclear spins on the QPC conductance. They observed hysteresis in the source-drain voltage dependence of the differential conductance under magnetic fields, and attributed its origin to the dynamical nuclear spin polarization (DNSP) induced in the QPC. However, NMR or other direct evidence showing involvement of nuclear spins has not been presented so far. NMR signal detection in the QPC conductance would constitute a novel experimental technique to probe spin properties of QPCs or nanowires[32, 33].

In this Letter, we report an electronic magnetization measurement of a QPC defined in a GaAs/AlGaAs heterostructure based on NMR spectroscopy. We find that the QPC differential conductance changes when the frequency of an applied oscillating magnetic field matches the NMR frequencies of ^{69}Ga , ^{71}Ga , and ^{75}As . The resistive detection of the NMR signals allows us to measure the electronic magnetization of the QPC from the Knight shifts of the NMR spectra. The Knight shift measurements are conducted at the QPC conductance between 0 and $2e^2/h$ by tuning gate and source-drain voltages. The magnetization changes smoothly with the QPC potential barrier height and peaks at the conductance plateau of $0.5 \times 2e^2/h$. The observed features are well captured by a model calculation assuming a smooth potential barrier without a bound state formed. Apart from the demonstration of a new technique to measure a magnetization of only a few electrons, the absence of a bound state in the QPC is our main conclusion, directly relevant for the understanding of the 0.7 structure.

QPCs studied in this work are fabricated from a wafer of GaAs/Al_{0.3}Ga_{0.7}As single heterostructure with a 2DES at the interface. The mobility and sheet carrier density of the 2DES at 4.2 K are 110 m²/Vs and $2.2 \times 10^{15} \text{ m}^{-2}$, respectively. A QPC is defined electrostatically applying negative voltages (V_{g1} , V_{g2}) to a pair

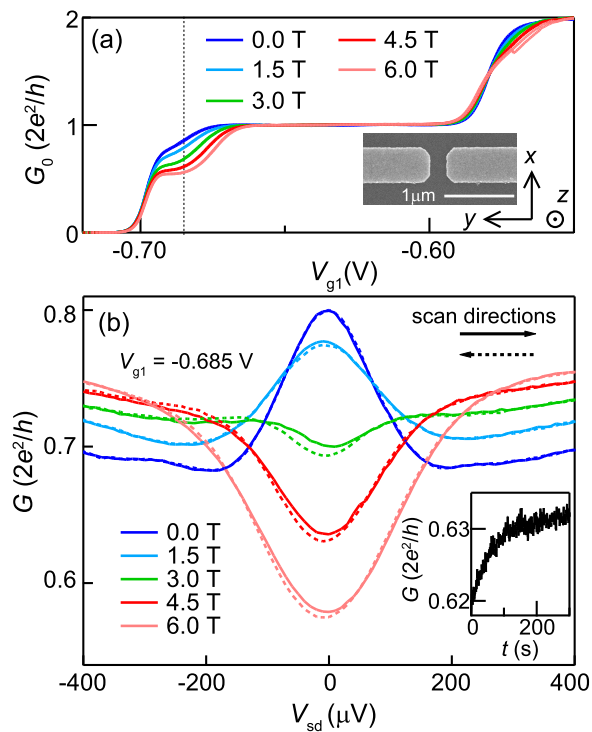


FIG. 1. (color online) (a) Linear conductance G_0 as a function of V_{g1} ($V_{g2} = -1.4$ V) at $B = 0, 1.5, 3, 4.5,$ and 6 T, applied along the x direction. Inset shows a scanning electron microscope image of the device. (b) Differential conductance G as a function of source-drain bias voltage V_{sd} at $V_{g1} = -0.685$ V [indicated by a dashed line in (a)] under the same magnetic fields as in (a). The solid (dashed) curves are measured by scanning V_{sd} in the positive (negative) direction at a rate of $5.6 \mu\text{V/s}$. Inset shows the time dependence of G at $B = 4.5$ T and $V_{g1} = -0.685$ V after an instantaneous change of V_{sd} from 0 to $-50 \mu\text{V}$. A slightly different value compared to the one in (b) for the same parameters, $B = 4.5$ T and $V_{sd} = -50 \mu\text{V}$, arises due to a remaining DNSP created at large $|V_{sd}|$ during the V_{sd} scan in (b).

of Au/Ti gate electrodes patterned on the surface of the wafer. All data presented here are measured on a QPC with lithographic dimensions of 300 nm length and 250 nm width [inset of Fig. 1(a)], in a dilution refrigerator at the mixing chamber temperature of 20 mK. The external magnetic field B is applied parallel to the 2DES plane along the current flowing direction [x direction in the inset of Fig. 1(a)] to avoid orbital effects and quantum Hall edge channels. The differential conductance $G = dI/dV_{sd}$ (where I is the current and V_{sd} is the source-drain bias voltage) is measured using a standard lock-in technique with a typical excitation voltage of $20 \mu\text{V}$ at 118 Hz. A single-turn coil is wound around the device to apply radio-frequency oscillating magnetic field B_{rf} .

The QPC shows a typical conductance quantization behavior. Figure 1(a) shows linear conductance $G_0 = G(V_{sd} = 0)$ as a function of gate voltage V_{g1} . In addi-

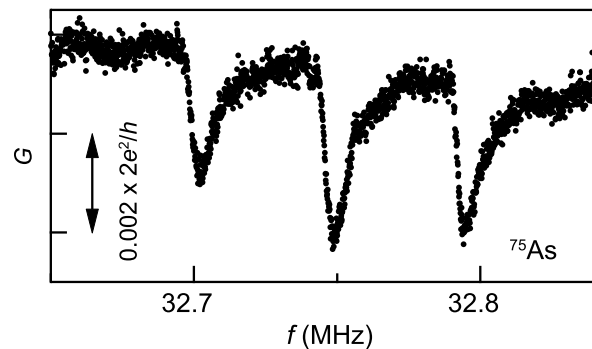


FIG. 2. Differential conductance G as a function of frequency f of B_{rf} at $B = 4.5$ T, $V_{g1} = -0.685$ V, and $V_{sd} = -50 \mu\text{V}$. B_{rf} is applied perpendicular to B [y direction in the inset of Fig. 1(a)]. f is scanned at a rate of 0.128 kHz/s. Data of 10 subsequent measurements are averaged to improve the signal to noise ratio.

tion to quantized conductance plateaus, the 0.7 structure is observed at zero magnetic field, developing into a plateau of $0.5 \times 2e^2/h$ at high magnetic fields. A zero-bias conductance peak accompanying the 0.7 structure is observed clearly in the G - V_{sd} curve at $B = 0$ T [Fig. 1(b)]. With increasing B , the zero-bias conductance peak is suppressed and turns into a dip above $B = 3$ T.

Hysteresis is observed in the G - V_{sd} curves when V_{sd} is scanned slowly ($5.6 \mu\text{V/s}$) in the positive and negative directions [Fig. 1(b)]. The hysteresis is seen only at finite magnetic fields. Typical time scale to develop the hysteresis is measured at $B = 4.5$ T by recording G after an instantaneous change of V_{sd} from 0 to $-50 \mu\text{V}$ [Inset of Fig. 1(b)]. The value of G continues to change over a period of 200 s. This time scale is consistent with nuclear spin relaxation or polarization times reported in GaAs-based devices[27, 28, 31, 34, 35]. Similarly as concluded in the earlier work[31], we interpret the slow change in G as the first indication for the DNSP in the QPC.

To confirm the nuclear spin origin of the observed slow change in G , we perform the NMR spectroscopy experiment. Scanning the frequency f of B_{rf} , we observe decreases in G when f matches the NMR frequency of ^{75}As (gyromagnetic ratio $\gamma = 45.82$ rad MHz/T) [Fig. 2]. The obtained G - f curve represents the NMR spectrum of ^{75}As , split into three dips due to the electric quadrupole interaction[36]. We observe signals at resonances of ^{69}Ga and ^{71}Ga , as well as analogous behavior in four other QPC devices (not shown). These observations clearly show that the DNSP is induced in the QPC and that its changes are measured by monitoring the QPC conductance.

Having established the method to probe the NMR spectra in transport, we now use it to determine the electronic magnetization of the QPC. To this end, we perform the following pump-probe experiment [Fig. 3(a)].

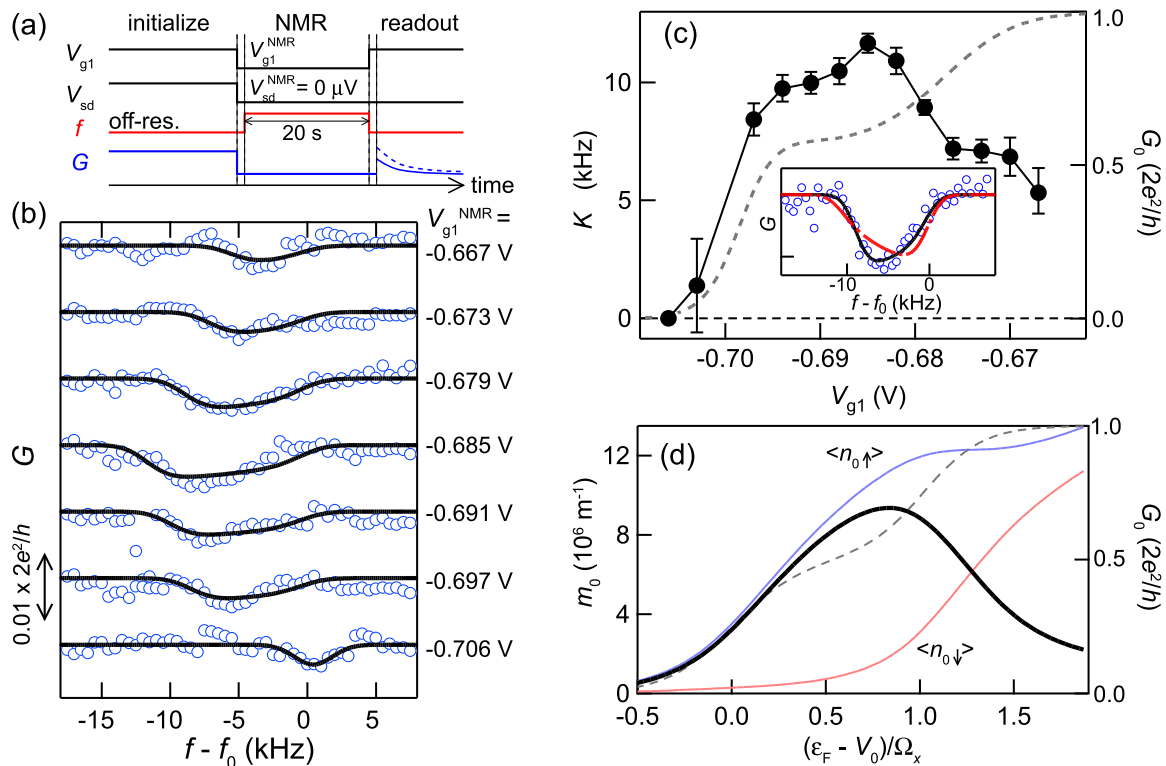


FIG. 3. (color online) (a) Schematic sequence for the pump-probe experiment. (b) NMR spectra of ^{75}As for $V_{sd}^{\text{NMR}} = 0 \mu\text{V}$ and various gate voltages V_{g1}^{NMR} , as indicated. NMR signals corresponding to the transition between nuclear spin states $|I_z = \pm 1/2\rangle$ are shown. Solid curves are the fitting results. Data are offset vertically for clarity. (c) Knight shift K plotted as a function of gate voltage V_{g1} . Linear conductance G_0 is plotted by a dotted curve referring to the right axis. Inset shows fitting results of the NMR data for $V_{g1}^{\text{NMR}} = -0.679 \text{ V}$ assuming 3D (dashed) and 2D (solid) hard-wall confinement potentials. (d) Calculated magnetization density at the QPC center m_0 plotted as a function of potential barrier height V_0 . The red and blue curves depict spin densities $\langle n_{0,\uparrow} \rangle$ and $\langle n_{0,\downarrow} \rangle$, respectively. Calculated conductance G_0 is plotted by a dotted curve referring to the right axis.

First, nuclear spins are initialized by inducing DNSP under a relatively large bias voltage $V_{sd} = -300 \mu\text{V}$ at $V_{g1} = -0.685 \text{ V}$. Then, V_{sd} is set to $0 \mu\text{V}$ and the QPC is tuned to a state of interest by setting the gate voltage to V_{g1}^{NMR} for a period of time (22 s), during which the frequency of B_{rf} is set to f for 20 s[37]. Finally, changes in the DNSP are read out by recording G with a small ac voltage excitation ($20 \mu\text{V}$, 118 Hz) at $V_{g1} = -0.685 \text{ V}$ and $V_{sd} = 0 \mu\text{V}$. The observed values of G at the beginning of the readout step reflect how much are the nuclear spins depolarized by B_{rf} . Repeating this procedure with different f , we obtain an NMR spectrum for a gate voltage V_{g1}^{NMR} as shown in Fig. 3(b).

The bottom data of Fig. 3(b) is obtained by depleting electrons from the QPC during the B_{rf} application. Therefore, this spectrum is not affected by electrons, and has a rather sharp dip at $f_0 = 32.755 \text{ MHz}$, the frequency corresponding to the transition between the nuclear spin states $|I_z = \pm 1/2\rangle$. As V_{g1}^{NMR} is increased, the NMR induced dips are shifted toward negative frequencies and broadened. These shifts are the Knight shifts due to the

electronic magnetizations in the QPC.

We now evaluate the magnitude of the Knight shifts by taking the spatial electron distribution into account. Extending earlier works[21, 22, 42], we adopt a model of electrons confined in the y and z directions with a transverse wave function $\psi(y, z)$. The Knight shift for an As nucleus at position (y, z) can be written as $\delta f_K(y, z) = \alpha_{\text{As}} m_z |\psi(y, z)|^2$, where $\alpha_{\text{As}} = -2.1 \times 10^{-22} \text{ kHz m}^3$ is the hyperfine coupling coefficient[36], and $m_z \equiv n_{\uparrow} - n_{\downarrow}$ is 1D electronic magnetization density defined as the difference in 1D spin densities. We make a standard assumption[42] that nuclear spins are depolarized by the rf-magnetic field according to the detuning from the resonance $\delta f = f - (f_0 + \delta f_K)$ with a Gaussian profile $\exp(-\delta f^2/2\gamma^2)$, where f_0 and γ are the NMR frequency and the spectrum width without the influence of the Knight shift, respectively. Such depolarizations induce the change in the electron Zeeman energy which is given by an integral of local nuclear spin depolarization multiplied by electron distribution. Since these changes are small, we may expand the QPC conductance, which

is a function of the electron Zeeman energy, and get for its change

$$\delta G(f) = A \int dydz \exp(-\delta f^2/2\gamma^2) |\psi(y, z)|^2, \quad (1)$$

with A an unknown proportionality coefficient. To evaluate Eq. (1), we approximate the transverse wave function by the one of a two-dimensional (2D) hard-wall confinement, $\psi(y, z) \propto \cos(\pi y/w_y) \cos(\pi z/w_z)$ with confinement widths $w_y = (65 \pm 5)$ nm and $w_z = (18 \pm 3)$ nm[43]. The Knight shift becomes $\delta f_K(y, z) = -K \cos^2(\pi y/w_y) \cos^2(\pi z/w_z)$ with a parameter K proportional to m_z via $K = -\alpha_{As} m_z |\psi(0, 0)|^2$. The experimental data in Fig. 3(b) are fitted to Eq. (1) using K and A as fitting parameters with $f_0 = 32.755$ MHz and $\gamma = 1.36$ kHz determined from the data measured at the depletion configuration ($V_{g1}^{\text{NMR}} = -0.706$ V). As seen in the figure, the agreement of the data and the model fitted for each curve is excellent.

We now consider an alternative fit, assuming that the QPC transport occurs through a three-dimensionally (3D) confined electronic state $\psi(x, y, z) \propto \cos(\pi x/w_x) \cos(\pi y/w_y) \cos(\pi z/w_z)$. A representative result, using an analog of Eq. (1), is given in the inset of Fig. 3(c) and shows a much worse compatibility with the data. We find that such discrepancy is not sensitive to the confinement details. As especially well visible for large Knight shifts, the data show skewed line shape, with steep (gentle) slopes on the low (high) frequency side. This is systematically reproduced by 2D confinement models, unlike 3D ones (see the Supplemental Material[36]).

In Fig. 3(c), K is plotted as a function of V_{g1} . A finite K emerges near the conductance onset and increases steeply as the conductance is increased to $0.5 \times 2e^2/h$. It keeps increasing gradually with increasing V_{g1} even in the conductance plateau region of $0.5 \times 2e^2/h$. As V_{g1} is increased further, K turns to decrease accompanied by a rise of conductance from $0.5 \times 2e^2/h$. As a result, a peak in K is formed at the high gate-voltage end of the conductance plateau. Using the relation between K and m_z , the observed maximum value $K = (11.7 \pm 0.5)$ kHz corresponds to $m_z = (16.5 \pm 4.5) \times 10^6 \text{ m}^{-1}$.

We now show that the observed features are well reproduced by a model calculation. We model a QPC by a 1D tight-binding Hamiltonian,

$$H = \sum_{j,\sigma} \epsilon_{j,\sigma} c_{j,\sigma}^\dagger c_{j,\sigma} - t \sum_{j,\sigma} c_{j,\sigma}^\dagger c_{j+1,\sigma} + \sum_j U_j n_{j,\uparrow} n_{j,\downarrow}. \quad (2)$$

Here $c_{j,\sigma}^\dagger$ creates an electron with spin σ ($\sigma = \uparrow, \downarrow$) at the j -th site of the tight-binding chain which has a hopping amplitude t . We assume a short-range Coulomb interaction represented by the on-site Coulomb energy U_j . The potential energy and the Zeeman energy are included in the on-site energy, $\epsilon_{j,\uparrow/\downarrow} = \epsilon_j \pm g\mu_B B/2$, with the Bohr

magneton μ_B and the electron g -factor g . We assume a smooth parabolic potential barrier at the QPC center with a height V_0 and a curvature Ω_x . The interaction term is treated by a mean-field approximation neglecting spin fluctuations. Then the mean-field spin density $\langle n_{j,\sigma} \rangle$ is determined by a self-consistent Green's function method[45], where the on-site energy $\epsilon_{j,\sigma}$ is shifted by $U_j \langle n_{j,\bar{\sigma}} \rangle$ with $\bar{\sigma}$, the opposite spin to σ . We calculate the magnetization density profile $m_j = \langle n_{j,\uparrow} - n_{j,\downarrow} \rangle$ and the QPC conductance G_0 . The values of U_j and Ω_x are determined from the conductance measurement data[36].

The thick solid curve in Fig. 3(d) depicts the calculated magnetization density at the QPC center $m_0 = m_{j=0}$ as a function of V_0 , resembling the observed V_{g1} dependence of K in Fig. 3(c). According to the calculation, the increase in m_0 accompanied by the emergence of the conductance corresponds to the increase in the number of up-spin electrons in the QPC. The value of m_0 starts to decrease when down-spin electrons begin to populate the QPC, lifting G_0 from $0.5 \times 2e^2/h$. The gradual increase in m_0 in the $0.5 \times 2e^2/h$ plateau region is also reproduced. The maximum value of the calculated magnetization density $m_0 = 9.3 \times 10^6 \text{ m}^{-1}$ roughly agrees with the value determined from the Knight shift. Spin polarization $P = \langle n_{0,\uparrow} - n_{0,\downarrow} \rangle / \langle n_{0,\uparrow} + n_{0,\downarrow} \rangle$ reaches 70.0 % where m_0 is maximal. Distribution of m_j has a bell-shaped profile and extends over a length of about 100 nm around the QPC center[36].

The gradual change in m_0 reflects the fact that the local density of states is continuous at the QPC center unlike in a quantum dot. We therefore attribute the observed gradual change in K to be consistent with a QPC model without any bound states. This contradicts earlier observations claiming that a single electron spin is trapped in a bound state formed in the QPC[14]. We estimate[36] that the observed magnitude of the magnetization density corresponds to the total magnetic moment (1.65 ± 0.45) in the QPC, exceeding the single-electron-spin magnetic moment which a bound state can support. Our measurement results of the NMR line shapes, the gradual change of K , and the magnetic moment values are consistent with a QPC model without bound states, such as Refs. [12, 13], which predicts a smooth increase of the magnetization without saturation upon increasing the magnetic field.

In summary, we find that the NMR signals can be detected by measuring the QPC conductance under in-plane magnetic fields. The resistive detection makes it possible to measure the electronic magnetization of the QPC from the Knight shifts of the NMR spectra. The electronic magnetization changes smoothly with the gate voltage and peaks at the conductance plateau of $0.5 \times 2e^2/h$. The gate voltage dependence of the Knight shift is well explained by a model calculation assuming a smooth potential barrier, supporting a no bound state origin of the 0.7 structure.

This work was supported partially by Grant-in-Aid for Scientific Research (No. 24684021) from JSPS, Japan. We thank T. Machida for valuable discussions.

* minoru@riken.jp

- [1] D. A. Wharam *et al.*, J. Phys. C **21**, L209 (1988).
 [2] B. J. van Wees *et al.*, Phys. Rev. Lett. **60**, 848 (1988).
 [3] M. Buttiker, Phys. Rev. B **41**, 7906 (1990).
 [4] K. J. Thomas *et al.*, Phys. Rev. Lett. **77**, 135 (1996).
 [5] K. J. Thomas *et al.*, Phys. Rev. B **58**, 4846 (1998).
 [6] C. -K. Wang and K. -F. Berggren, Phys. Rev. B **57**, 4552 (1998).
 [7] D. J. Reilly *et al.*, Phys. Rev. B **63**, 121311 (2001).
 [8] K. A. Matveev, Phys. Rev. Lett. **92**, 106801 (2004).
 [9] S. M. Cronenwett *et al.*, Phys. Rev. Lett. **88**, 226805 (2002).
 [10] Y. Meir, K. Hirose and N. S. Wingreen, Phys. Rev. Lett. **89**, 196802 (2002).
 [11] T. Rejec and Y. Meir, Nature **442**, 900 (2006).
 [12] C. Sloggett, A. I. Milstein, and O. P. Sushkov, Eur. Phys. J. B **61**, 427 (2008).
 [13] F. Bauer *et al.*, Nature **501**, 73 (2013).
 [14] Y. Yoon *et al.*, Phys. Rev. Lett. **99**, 136805 (2007).
 [15] L. DiCarlo *et al.*, Phys. Rev. Lett. **97**, 036810 (2006).
 [16] M. J. Iqbal *et al.*, Nature **501**, 79 (2013).
 [17] B. Brun *et al.*, Nature Commun. **5**, 4290 (2014).
 [18] L. W. Smith *et al.*, Phys. Rev. Lett. **107**, 126801 (2011).
 [19] A. P. Micolich, J. Phys. Condens. Matter **23**, 443201 (2011) and the references there in.
 [20] S. M. Grinolds *et al.*, Nature Phys. **9**, 215 (2013).
 [21] N. Kumada, K. Muraki, and Y. Hirayama, Phys. Rev. Lett. **99**, 076805 (2007).
 [22] L. Tiemann *et al.*, Science **335**, 828 (2012).
 [23] M. Stern *et al.*, Phys. Rev. Lett. **108**, 066810 (2012).
 [24] B. E. Kane, L. N. Pfeiffer, and K. W. West, Phys. Rev. B **46**, 7264 (1992).
 [25] K. R. Wald, L. P. Kouwenhoven, P. L. McEuen, N. C. van der Vaart, and C. T. Foxon, Phys. Rev. Lett. **73**, 1011 (1994).
 [26] D. C. Dixon, K. R. Wald, P. L. McEuen, and M. R. Melloch, Phys. Rev. B **56**, 4743 (1997).
 [27] S. Kronmuller *et al.*, Phys. Rev. Lett. **82**, 4070 (1999).
 [28] M. Kawamura *et al.*, Appl. Phys. Lett. **90**, 022102 (2007).
 [29] W. Desrat *et al.*, Phys. Rev. Lett. **88**, 256807 (2002).
 [30] C. P. Slichter, *Principles of Nuclear Magnetism* (Oxford University Press, New York, 1984).
 [31] Y. Ren, W. Yu, S. M. Frolov, J. A. Folk, and W. Wegscheider, Phys. Rev. B **81**, 125330 (2010).
 [32] N. R. Cooper and V. Tripathi, Phys. Rev. B **77**, 245324 (2008).
 [33] P. Stano and D. Loss, Phys. Rev. B **90**, 195312 (2014).
 [34] M. Kawamura *et al.*, Phys. Rev. B **79**, 193304 (2009).
 [35] M. Kawamura, D. Gottwald, K. Ono, T. Machida, and K. Kono, Phys. Rev. B **87**, 081303 (2013).
 [36] See the Supplemental Material which includes Refs. [38–41] at http://link.aps.org/**/ for the details of electric quadrupole splitting, stability of external magnetic field, determination of the hyperfine coupling constant α_{As} , alternative fitting analysis, and the tight-binding model calculation.
 [37] The small ac voltage V_{ac} (20 μ V, 118 Hz) was not turned off during this period of 22 s. Although the small V_{ac} might induce the DNSP, its amplitude is much smaller than that induced by $V_{sd} = -300\mu$ V at the first step.
 [38] K. A. Dumas, J. F. Soest, A. Sher, and E. M. Swiggard, Phys. Rev. B **20**, 4406 (1979).
 [39] D. Paget *et al.*, Phys. Rev. B **15**, 5780 (1977).
 [40] J. Schliemann, A. Khaetskii, and D. Loss, J. Phys. Condens. Matter **15**, R1809 (2003).
 [41] T. Ando, Phys. Rev. B **44**, 8017 (1991).
 [42] P. Khandelwal, N. N. Kuzma, S. E. Barrett, L. N. Pfeiffer, and K. W. West, Phys. Rev. Lett. **81**, 673 (1998).
 [43] The parameter $w_z = (18 \pm 3)$ nm is typical for the interface of GaAs/AlGaAs[44]. The parameter $w_y = (65 \pm 5)$ nm, which is related to the inter-subband energy, is determined from the gate voltage width of the first conductance plateau.
 [44] T. Ando, J. Phys. Soc. Jpn. **51**, 3900 (1982).
 [45] S. Datta, *Quantum Transport: Atom to Transistor* (Cambridge University Press, Cambridge, England, 2005).

Supplementary Material on
**Electronic magnetization of a quantum point contact
measured by nuclear magnetic resonance**

Electric quadrupole splitting of the NMR spectra

The NMR spectrum of ^{75}As shown in Fig. 2 of the main text is split into three conductance dips. Similarly the spectra for ^{69}Ga and ^{71}Ga constitute of three conductance dips as respectively shown in Figs. S1(a) and (b). These splittings are due to the electric quadrupole interaction, the interaction between the electric quadrupole moment of the nuclei and the electric field gradient at the position of the nuclei. The amplitude of the electric quadrupole interaction, hence the amplitude of splittings, is expected to be proportional to the electric quadrupole moment of nuclei. The observed amplitudes of the NMR spectrum splittings are $\Delta f = 47$ kHz, 23 kHz, and 15 kHz for ^{75}As , ^{69}Ga , and ^{71}Ga , respectively. The ratio of the Δf roughly agrees with the ratio of the electric quadrupole moment Q in literature[1]; $Q_{^{75}\text{As}} = 0.29 \times 10^{-28} \text{ m}^2$, $Q_{^{69}\text{Ga}} = 0.19 \times 10^{-28} \text{ m}^2$, and $Q_{^{71}\text{Ga}} = 0.12 \times 10^{-28} \text{ m}^2$. In a cubic symmetric bulk GaAs crystal, the electric quadrupole interaction is usually zero. We infer that the strain induced by the pair of Ti/Au gate electrodes breaks the cubic symmetry and induces the electric quadrupole splittings in the observed NMR spectra.

Stability of external magnetic field

The NMR spectra shown in Fig. 3(b) of the main text are taken at $B = 4.5$ T. The magnetic field is produced by a superconducting solenoid using a persistent mode and the field is not changed throughout the series of the measurements. It took about 80 hours to complete the set of the NMR spectra under various gate voltages shown in Fig. 3(b). We took the data for $V_{\text{g1}}^{\text{NMR}} = -0.685$ V twice after an interval of about 50 hours and confirmed that the frequency shift was less than 1.5 kHz. This indicates that the magnetic field was stable enough to resolve the Knight shift of the QPC.

Hyperfine coupling constant

Hyperfine interaction between a nuclear spin \vec{I}_i and electron spins \vec{s}_j is described by a Hamiltonian

$$H(\vec{I}_i) = \sum_j \frac{4\mu_0}{3I} \mu_B \mu_X |\Psi_j(\vec{R}_i)|^2 \vec{s}_j \cdot \vec{I}_i. \quad (1)$$

Here μ_0 is a magnetic permeability, μ_B is the Bohr magneton, and μ_X is the magnetic moment of the nucleus which depends on the isotope X . $\Psi(\vec{R}_i)$ is the electronic wave function amplitude at the location \vec{R}_i of the nucleus. In a semiconductor crystal, this wave function is a product of a periodic atomic wave function $u(\vec{r})$, and an envelope function $\psi_j(\vec{r})$, namely $\Psi_j(\vec{r}) = \psi_j(\vec{r})u(\vec{r})$. Then we can rewrite the Hamiltonian as

$$H(\vec{I}_i) = \mu_X \left(\sum_j \frac{4\mu_0}{3I} \mu_B \eta_X |\psi_j(\vec{R}_i)|^2 \vec{s}_j \right) \cdot \vec{I}_i = \mu_X \vec{B}_K \cdot \vec{I}_i \quad (2)$$

with $\eta_X = |u(\vec{R}_i)|^2$. Values of η_X depend on nuclear species as well as the crystal structure. When electrons are polarized, the sum is not zero and results in an effective magnetic field (Knight field) \vec{B}_K acting on the nuclear spin \vec{I}_i , leading to the Knight energy shift of $\mu_X |\vec{B}_K|$, equivalent to a frequency shift $\delta f_K = \mu_X |\vec{B}_K| / h$.

For 1D electrons confined in the y and z directions, the Knight shift has a spatial variation reflecting the envelope function profile,

$$\delta f_K(y, z) = \alpha_X (n_{\uparrow}^{1D} - n_{\downarrow}^{1D}) |\psi(y, z)|^2 = \alpha_X m_{1D} |\psi(y, z)|^2, \quad (3)$$

where $\alpha_X \propto \mu_X \eta_X$ is a nuclear-species dependent coupling coefficient, n_{\uparrow}^{1D} and n_{\downarrow}^{1D} are spin-resolved 1D electron densities, and $m_z^{1D} \equiv n_{\uparrow}^{1D} - n_{\downarrow}^{1D}$ is the 1D magnetization density. Assuming for simplicity a hard-wall

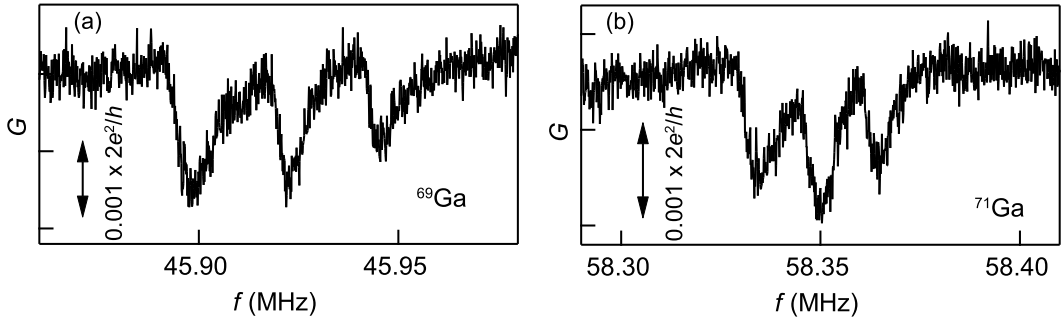


FIG. S1 . Response of differential conductance G to rf-magnetic field B_{rf} plotted as a function of frequency f . Frequency ranges corresponding to NMR spectra for ^{69}Ga (a) and ^{71}Ga (b) are shown, respectively. The data are obtained at the same condition as Fig. 2 of the main text ($B = 4.5$ T, $V_{g1} = -0.685$ V, and $V_{\text{sd}} = -50$ μV).

confinement in the QPC cross-section, the transversal ground state (lowest subband) wave function is $\psi(y, z) = \sqrt{2/w_y} \sqrt{2/w_z} \cos(\pi y/w_y) \cos(\pi z/w_z)$ with confinement widths w_y and w_z . Then the maximum value of the Knight shift K becomes

$$K = \alpha_X m_{1\text{D}} \left(\frac{2}{w_y} \right) \left(\frac{2}{w_z} \right). \quad (4)$$

Similarly, in the case of 2D electron system confined in the z direction, the Knight shift becomes

$$K = \alpha_X (n_{\uparrow}^{2\text{D}} - n_{\downarrow}^{2\text{D}}) \left(\frac{2}{w_z} \right) = \alpha_X m_{2\text{D}} \left(\frac{2}{w_z} \right), \quad (5)$$

using the same coefficient α_X as in the 1D case. Here $n_{\uparrow}^{2\text{D}}$ and $n_{\downarrow}^{2\text{D}}$ are spin-resolved 2D electron densities, and $m_z^{2\text{D}} \equiv n_{\uparrow}^{2\text{D}} - n_{\downarrow}^{2\text{D}}$ is the 2D magnetization density. Based on the Knight shift measurements in GaAs quantum wells with 2D electron systems, the coefficient for $X = ^{71}\text{Ga}$ is reported as $\alpha_{71\text{Ga}} = -(4.5 \pm 0.2)/2 \times 10^{-22}$ kHz m^3 [2] (This is half the original value in Ref. [2] because of the difference in the definition of α). The negative sign means that negative frequency shift is induced by up-spin electrons. Putting this value and values for μ_X and η_X ($\mu_{71\text{Ga}} = 2.562 e\hbar/2m_p$, $\mu_{75\text{As}} = 1.439 e\hbar/2m_p$, $\eta_{71\text{Ga}} = 2.7 \times 10^3$, and $\eta_{75\text{As}} = 4.5 \times 10^3$ [3, 4]) into a proportionality relation

$$\frac{\alpha_{75\text{As}}}{\alpha_{71\text{Ga}}} = \left(\frac{\mu_{75\text{As}}}{\mu_{71\text{Ga}}} \right) \left(\frac{\eta_{75\text{As}}}{\eta_{71\text{Ga}}} \right), \quad (6)$$

the coefficient for ^{75}As is determined as $\alpha_{75\text{As}} = -2.1 \times 10^{-22}$ kHz m^3 .

Fitting results with various confinement potentials

In the main text, we state that a 3D confinement model can not be reconciled with the measured data. Here we demonstrate that this conclusion is insensitive to the wave function shape, and therefore the precise confinement profile. To this end, we fit the NMR spectra [Fig. 3(b) of the main text] using various wave function profiles at around the center of the QPC. We assume that the conductance is a function of the Zeeman energy. Because the change in the Zeeman energy δE_z induced by the rf-magnetic field is small, we can expand the conductance to find its change $\delta G(f)$ being proportional to δE_z . The change δE_z can be written by an integral of the local Overhauser field change $\delta B_N(\vec{r}; f)$ multiplied by electron distribution $|\psi(\vec{r})|^2$ with an unknown proportionality coefficient A . Then δG can be written as

$$\delta G(f) \propto \delta E_z \quad (7)$$

$$= A \int d\vec{r} \delta B_N(\vec{r}; f) |\psi(\vec{r})|^2 \quad (8)$$

$$= A \int d\vec{r} I[f - (f_0 + \delta f_K(\vec{r}), \gamma)] |\psi(\vec{r})|^2, \quad (9)$$

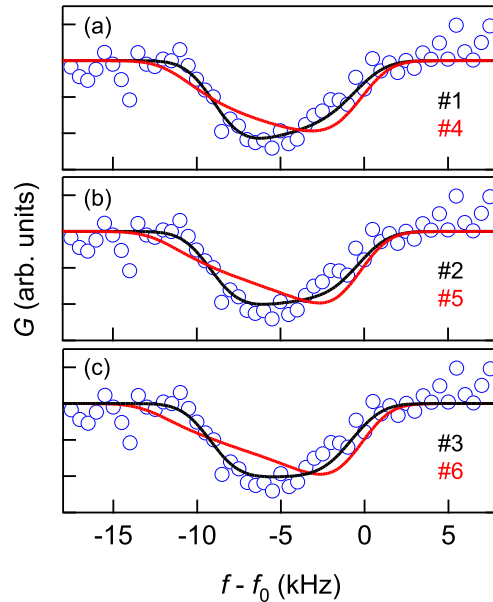


FIG. S2 . Fitting results to the NMR data, from Fig. 3(b) in the main text, for $V_{g1}^{\text{NMR}} = -0.679$ V assuming 6 different wave function profiles. The wave function profiles are listed in Table I. (a) The results for #1 (black) and #4 (red). (b) The results for #2 (black) and #5 (red). (c) The results for #3 (black) and #6 (red). The yielded fitting parameters are $K = 8.9, 9.2, 9.2, 11.3, 12.1,$ and 13.0 kHz and $A = -4.6 \times 10^{-5}, -4.0 \times 10^{-5}, -3.4 \times 10^{-5}, -1.6 \times 10^{-6}, -1.2 \times 10^{-6},$ and -1.4×10^{-6} for #1 - #6, respectively (The wave function pre-factor C is chosen so that $\text{Max}\{|\psi|^2\} = 1$).

Index	Wave function profile	Potential
#1	$C \cos(\pi y/w_y) \cos(\pi z/w_z)$	2D hard-wall
#2	$C \exp(-y^2/2l_y^2) \cos(\pi z/w_z)$	parabolic (y) and hard-wall (z)
#3	$C \exp(-y^2/2l_y^2) \text{Ai}(z/l_z + n_0)$	parabolic (y) and triangular (z)
#4	$C \cos(\pi x/w_x) \cos(\pi y/w_y) \cos(\pi z/w_z)$	3D hard-wall
#5	$C \exp(-x^2/2l_x^2) \exp(-y^2/2l_y^2) \cos(\pi z/w_z)$	parabolic (x, y) and hard-wall (z)
#6	$C \exp(-x^2/2l_x^2) \exp(-y^2/2l_y^2) \text{Ai}(z/l_z + n_0)$	parabolic (x, y) and triangular (z)

TABLE I. Wave function profiles used for the fitting analysis and the corresponding confinement potentials. $\text{Ai}(z)$ and n_0 denote the Airy function and its largest zero point, respectively. The parameters are $w_x = w_y = 60$ nm, $w_z = 15$ nm, $l_x = l_y = 19.8$ nm, and $l_z = 5.5$ nm.

where $\delta f_K(\vec{r}) = \alpha_{\text{As}} m_z |\psi(\vec{r})|^2$ is the Knight shift at the position \vec{r} . A Gaussian function $I(\delta f, \gamma) = \exp(-\delta f^2/2\gamma^2)$ describes the depolarization of nuclear spins by rf-magnetic field at a frequency detuning $\delta f \equiv f - (f_0 + \delta f_K)$ with f_0 being the NMR frequency without the influence of the Knight shift. Rewriting $\delta f_K(\vec{r}) = -K |\psi(\vec{r})|^2 / \text{Max}\{|\psi(\vec{r})|^2\}$ and using K and A as fitting parameters, the experimental data in Fig. 3(b) in the main text are fitted to Eq. (9) with $f_0 = 32.755$ MHz and $\gamma = 1.36$ kHz, the same as in the main text.

For the fitting analysis, we assume 6 different wave function profiles $\psi(\vec{r})$ listed in table I. The fitting results to the $V_{g1}^{\text{NMR}} = -0.679$ V data are shown in Fig. S2. The wave function profiles #1 - #3 correspond to a 2D confinement potential supposing that no bound state is formed at around the QPC center. The wave function profiles #4 - #6 correspond to a 3D confinement potential supposing that a bound state is formed around the QPC center. As seen in the figure, the correspondence is systematically much worse in the latter cases compared to the former ones. As a general feature, 3D confinement models result in gentle slopes on the low-frequency side and steep slopes on the high-frequency side regardless of the details of the wave function profiles. This trend is opposite to the experimentally observed spectrum shapes, especially for those with large Knight shifts, and 2D confinement models correctly gasp this behavior.

To understand this robust dependence of the conductance dip shape on the wave function confinement dimension-

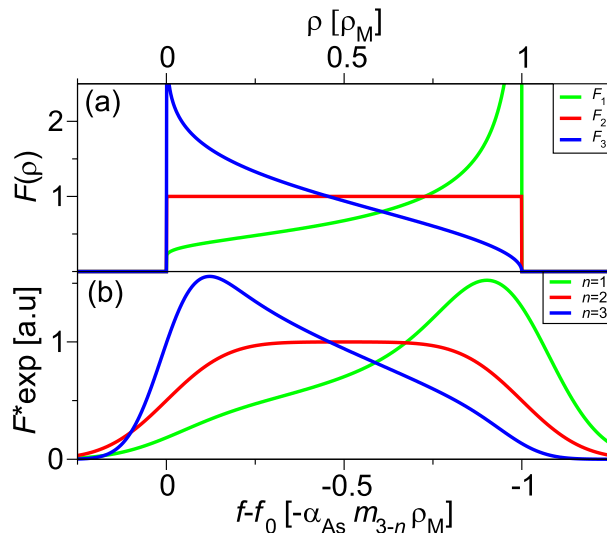


FIG. S3 . (a) The functions $F_n(\rho)$ in Eq. (10). (b) The convolution [Eq. (10)] evaluated numerically for parameters as given in the text for m_0 , m_1 , and $m_2 = m_1/20$ nm, $\alpha_{As} = -5 \times 10^{-22}$ kHz m³, $\gamma = 1.36$ kHz, $l_0 = 5.5, 10.5,$ and 13 nm for $n = 1, 2,$ and $3,$ respectively.

ality, we rewrite the spatial integral in Eq. (9) into an integral over the electron density $\rho = |\Psi|^2$,

$$\delta G(f) \propto \int_0^{\rho_M} d\rho F_n(\rho) \exp\left(-\frac{[f - f_0 - \alpha_{As} m_{3-n} \rho]^2}{2\gamma^2}\right), \quad (10)$$

where we introduce the magnetization densities for two ($n = 2$) and three ($n = 3$) dimensional confinement as $m_1 \equiv 16.5 \mu\text{m}^{-1}$ (our experiment) and $m_0 = 1$ (a polarized local moment), respectively. The distribution of the density ρ between its minimal $\rho = 0$ and maximal value $\rho = \rho_M$ is given by the weight function $F_n(\rho)$. For illustration, we take a spherically symmetric Gaussian density profile, $|\Psi(\vec{r})|^2 = \rho_M \exp(-r^2/l_0^2)$, for which $F_n(\rho)$ can be calculated analytically as $F_n(\rho) \propto [\ln(\rho_M/\rho)]^{(n-2)/2}$. This function is plotted on Fig. S3 (a), from where the dimensionality effect is clearly visible. Indeed, for $n = 2$ (red curves) the weight function is constant, so its convolution with the Gaussian frequency distribution will result in a symmetric profile, as shown on Fig. S3 (b). Compared to that, a three dimensionally confined wave function has more weight at small ρ , which in other words means that it has a more weight in the tail. This results in an asymmetric shape of the convolution, skewed to the left (blue curves). Because α_{As} is negative, the shape is mirror reflected when converting the horizontal axis from the Knight shift in Fig. S3 (a) to the NMR frequency in Fig. S3 (b) and Fig. S2. This allows us to exclude the possibility of a 3D confinement model, as our data systematically show either symmetric, or skewed towards lower frequencies shapes, corresponding to 2D, and 1D confinement models, respectively.

We also note that the black curves (#1 - #3) in Fig. S2 look very similar, suggesting that the fitting does not depend strongly on the details of the wave function profiles, and yield robust values of K , being 8.9 kHz, 9.2 kHz, and 9.3 kHz for #1, #2, and #3, respectively. There is a recognizable trend, namely the values of K tend to increase as the tails of the wave function profile extends. Therefore the model of the 2D hard-wall potential we adopt in the main text gives a bound from below for K , hence for m_z which already exceeds the magnetic moment for a single electron spin. This further corroborates that our conclusions are not artifacts of a specific confinement model.

Model calculation

In our tight-binding model calculation, we assume a smooth parabolic potential barrier at the center of the QPC with a height V_0 and a curvature Ω_x . Intermediate regions ($j_0 < |j| \leq N$) are inserted between the central part of the QPC and the leads, where $\epsilon_j = 0$, to connect the potential smoothly [Fig. S4(a)][5];

$$\epsilon_j = \begin{cases} V_0 - \frac{\Omega_x^2}{4t} j^2, & |j| \leq j_0 \\ a(j - N)^2 + b(j - N)^4, & j_0 < |j| \leq N \\ 0, & N < |j| \end{cases}, \quad (11)$$

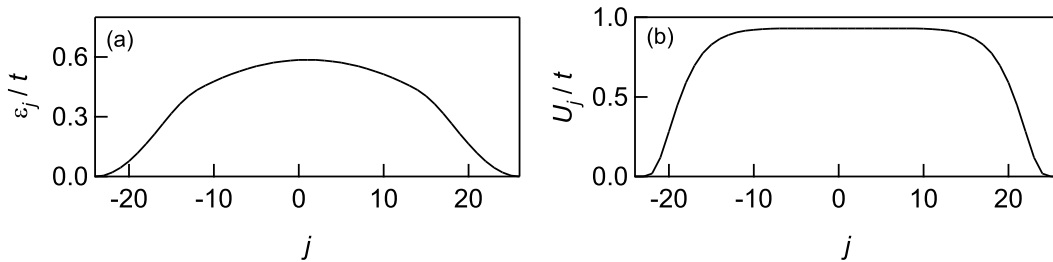


FIG. S4 . Tight-binding model parameters for $N = 25$, $j_0 = 13$, $\Omega_x/t = 0.078$, $V_0/t = 0.586$, and $U/t = 0.93$. (a) Potential energy ϵ_j as a function of site index j . (b) Site dependent Coulomb interaction U_j as a function of j .

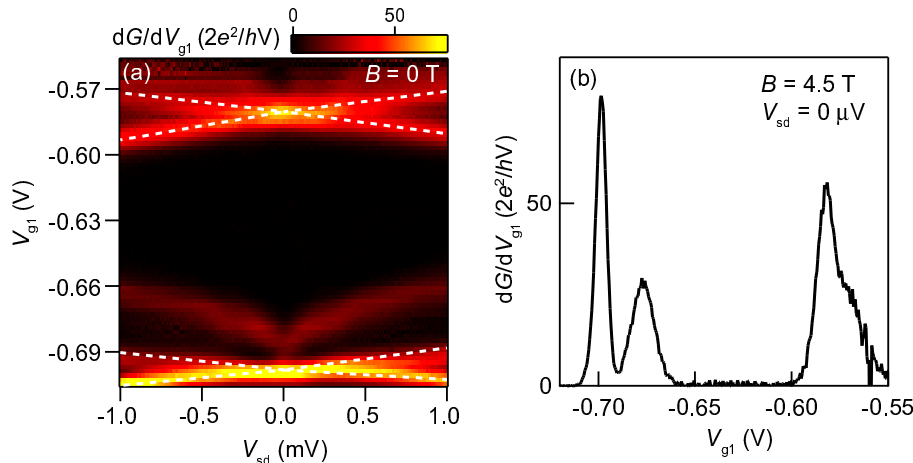


FIG. S5 . (color online) (a) Transconductance ($\partial G/\partial V_{g1}$) plotted in color scale as a function of V_{sd} and V_{g1} for $B = 0.0$ T. The dotted lines trace the alignment of subband edges with the source and drain electrochemical potentials. A lever-arm factor converting from gate voltage to energy is derived from their slopes and intersections. (b) Transconductance for $V_{sd} = 0$ μ V and $B = 4.5$ T plotted as a function of V_{g1} . The strength of Coulomb interaction U is set by requiring that the calculated result reproduces the measured energy difference between the spin-split transconductance peaks.

where a and b are determined so that ϵ_j and $d\epsilon_j/dj$ are continuous at $j = j_0$:

$$a = \frac{2}{(j_0 - N)^2} \left(V_0 - \frac{\Omega_x^2}{4t} j_0^2 + \frac{\Omega_x^2}{8t} j_0(j_0 - N) \right), \quad (12)$$

$$b = \frac{1}{4(j_0 - N)^2} \left(-\frac{\Omega_x^2}{2t} j_0^2 - 2a(j_0 - N) \right). \quad (13)$$

The on-site Coulomb energy U_j is non-zero only in the constriction part and changes smoothly to $U_j = 0$ in the lead [Fig. S4(b)] [5, 6].

$$U_j = \begin{cases} U \exp\left(-\frac{(j/N)^6}{1 - (j/N)^2}\right), & |j| \leq N \\ 0, & |j| > N. \end{cases} \quad (14)$$

The parameters for the model calculation are determined as follows. The hopping amplitude t is related to the Fermi energy ϵ_F by $\epsilon_F = 2t(1 - \cos 2\pi a/\lambda_F)$, where λ_F is the Fermi wave length and a is the lattice constant of the tight-binding chain. The numerical calculations are done for $N = 25$ and $j_0 = 13$. The lattice constant a is set to $a = 1/8\lambda_F$ [7], which leads to the QPC length of 340 nm for $N = 25$. A lever-arm factor $\eta = 34$ meV/V converting gate voltage V_{g1} to energy is extracted from the transconductance ($\partial G/\partial V_{g1}$) data in Fig. S5(a). Then, assuming a transmission probability $t_n(\epsilon) = 1/(1 + e^{2\pi(\epsilon_n - \epsilon)/\Omega_x})$ [8], the curvature of the potential barrier Ω_x is evaluated by fitting the linear conductance transition between $2e^2/h$ and $4e^2/h$. The parameter U is determined so that the calculated result reproduces the energy difference between the transconductance peaks corresponding to the spin-split

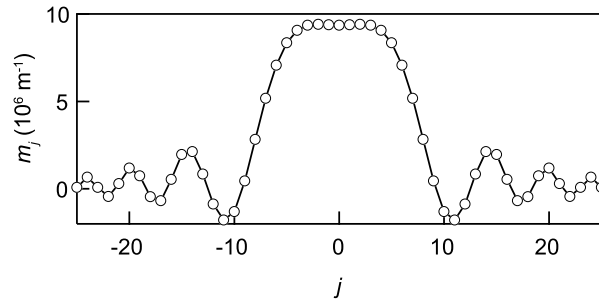


FIG. S6 . Calculated magnetization density m_j as a function of site index j for $(\epsilon_F - V_0)/\Omega_x = 0.82$ where $m_{j=0}$ is set to the maximal value observed in Fig. 3(d) of the main text.

conductance transitions [Fig. S5(b)]. For the QPC measured, we find $t = 12.8$ meV, $\Omega_x = 1.0$ meV and $U/t = 0.93$. The value of g -factor $|g| = 0.44$ for bulk GaAs is used for the Zeeman energy.

Figure S6 depicts the spatial distribution of the calculated magnetization density m_j for $(\epsilon_F - V_0)/\Omega_x = 0.82$ where $m_{j=0}$ is set to be maximal seen in Fig. 3(d) of the main text. The distribution is a bell-shaped curve at the QPC center with a length at half maximum of 16 sites which corresponds to the distribution length L of about 100 nm. We use the calculated L to convert the observed magnetization density m_z to the total magnetic moment M in the QPC, by $M = m_z L$. In this way we get the result stated in the main text, that the observed magnetization density of $m_z = (16.5 \pm 4.5) \text{ m}^{-1}$ corresponds to a total magnetic moment of $M = 1.65 \pm 0.45$.

-
- [1] K. A. Dumas, J. F. Soest, A. Sher, and E. M. Swiggard, Phys. Rev. B **20**, 4406 (1979).
 - [2] P. Khandelwal *et al.*, Phys. Rev. Lett. **81**, 673 (1998).
 - [3] D. Paget *et al.*, Phys. Rev. B **15**, 5780 (1977).
 - [4] J. Schliemann, A. Kaetskii, and D. Loss, J. Phys. Condens. Matter **15**, R1809 (2003).
 - [5] F. Bauer *et al.*, Nature **501**, 79 (2013).
 - [6] C. Sloggett, A. I. Milstein, and O. P. Sushkov, Eur. Phys. J. B **61**, 427 (2008).
 - [7] T. Ando, Phys. Rev. B **44**, 8017 (1991).
 - [8] M. Buttiker, Phys. Rev. B **41**, 7906 (1990).